Temperature dependence and capping and underlayer layers effect on the interfacial magnetic properties of Ir/Fe- or Pt/Fe-based systems

Djoudi Ourdani ◉,[1] N. Challab,[1] Yves Roussigné ◉,[1] Salim Mourad Chérif ◉,[1]
Mihai Sebastian Gabor ◉,[2,*] and Mohamed Belmeguenai ◉[1,†]

[1]*Université Sorbonne Paris Nord, LSPM, CNRS, UPR 3407, F-93430 Villetaneuse, France*
[2]*Center for Superconductivity, Spintronics and Surface Science, Physics and Chemistry Department, Technical University of Cluj-Napoca,
Strada Memorandumului No. 28, RO-400114 Cluj-Napoca, Romania*

Brillouin light scattering and microstrip line ferromagnetic resonance were used to study perpendicular magnetic anisotropy (PMA), magnetic damping, and interfacial Dzyaloshinskii-Moriya interaction (iDMI) in X/Fe(t_{Fe})/Y thin films with varying Fe thickness (1.4 nm $\leqslant t_{Fe} \leqslant$ 10 nm), where X stands for Pt, Ir, or Cu and Y stands for Ir, Cu, or MgO. A particular interest is given to their temperature dependence. To accurately assess the contribution of each interface with Fe to the effective interface PMA constant, we combined direct measurements of the effective magnetization thickness dependence with the spin waves frequency mismatch. Notably, Ir/Fe and Fe/Ir, as well as Cu/Fe and Fe/Cu interfaces exhibited distinct behaviors: Fe/Ir significantly contributed to PMA and spin pumping induced damping. The damping constant showed a nonlinear dependence on the Fe layer inverse effective thickness, which was linked to a strong interfacial two-magnon scattering, particularly evident in Cu/Fe/Ir and Cu/Fe/Cu structures. Additionally, iDMI measurements revealed an opposite chirality of Pt/Fe and Ir/Fe interfaces. We also investigated how these magnetic interfacial properties vary with temperature in the Pt/Fe/Cu and Cu/Fe/Cu systems. We found that the interface PMA constant increased linearly with temperature, while the iDMI constant decreased significantly, by approximately 60%. This suggests that iDMI is highly sensitive to thermal disorder. Post-temperature measurements indicated that the temperature induces interdiffusion and impacts the magnetic properties through specific effects that are challenging to disentangle in the absence of *in situ* magnetization measurements.

I. INTRODUCTION

The spin-orbit interaction, which couples the orbital motion of electrons to their spins, plays a key role in several important magnetic phenomena. Consequently, it offers a promising avenue for the creation of innovative spintronic devices [1]. Recent discoveries highlight that the interface between ferromagnetic material (FM) and heavy metal (HM) hosts a diverse range of significant phenomena linked to spin-orbit coupling. These phenomena include spin-orbit torque [2], interfacial perpendicular magnetic anisotropy (PMA) [3–5], spin pumping induced damping [6], interfacial Dzyaloshinskii-Moriya interaction (iDMI) [7], and spin-current generation [8]. Such phenomena are expected to play a crucial role in advancing the next generation of spintronic devices, characterized by an improved performance (faster and denser) with reduced power consumption, ultimately determining the feasibility and the success of these technologies.

iDMI is a relatively recent evidenced phenomenon that significantly influences the static and dynamic magnetic properties of FM/HM ultrathin film systems. It modifies the static

and dynamic behaviors of domain walls [9], induces nonreciprocal spin wave propagation [10], and gives rise to unique chiral and topological magnetic structures like magnetic spirals and skyrmions. Both *ab initio* calculations [11], focusing on ideal stacks, and experimental studies [12] support the view that iDMI represents an interface magnetic energy. The sign of iDMI is particularly important as it determines the chirality of the interface. Additionally, maximizing PMA is crucial for reducing the size of spintronic devices used in data storage and for stabilizing domain walls and skyrmions with varying chirality when combined with iDMI. Magnetic damping is another essential material parameter that plays pivotal roles in numerous spintronic applications. These magnetic material parameters need to be precisely defined and tuned based on the specific requirements of the intended application. Therefore, several HMs/FMs have undergone experimental testing. Given that the FM film has two interfaces, it can be challenging to isolate their individual contributions to PMA, iDMI, and damping in a given "bottom layer/FM/top layer" structure. Furthermore, the temperature exerts a significant influence on the magnetic properties of diverse materials, especially in the case of ultrathin films. Temperature not only offers an effective avenue for exploring the interplay between these parameters but also serves as a valuable tool for comprehending their physical origins and assessing the performance of spintronic devices under elevated temperatures. Moreover,

---
*Contact author: mihai.gabor@phys.utcluj.ro
†Contact author: belmeguenai.mohamed@univ-paris13.fr

it is expected that electronic devices might operate efficiently over a broader temperature range, extending beyond room temperature. Therefore, this paper focuses on exploring damping, PMA, and iDMI in Cu/Fe- and Pt/Fe-based systems, with special attention to effects of the temperature and the influence of underlayers and capping layers. Various material combinations and stacking orders are examined to identify the distinct contributions to PMA, iDMI, and damping. To achieve this, ferromagnetic resonance (FMR) and Brillouin light scattering (BLS) coupled with vibrating sample magnetometry (VSM) techniques were employed.

II. SAMPLES AND EXPERIMENTAL TECHNIQUES

The studied samples are 5×5 mm^2 in lateral size and consist of layers structured as follows: Si/SiO$_2$/Ta (2.5 nm)/X/Fe(t_{Fe})/Y/Ta (2.5 nm), where X stands for Pt (4 nm), Ir (4 nm), and Cu (2 nm), and Y includes Ir (4 nm), Cu (2 nm), and MgO (1 nm), with the Fe layer thickness (t_{Fe}) ranging from 1.4 to 10 nm. The samples were grown using a magnetron sputtering system with a base pressure lower than 2×10^{-8} Torr. The metallic layers were deposited using dc sputtering under an Ar pressure of 1.5 mTorr, while the 1 nm thick MgO layer was grown by rf sputtering in an Ar pressure of 10 mTorr. Hysteresis loops were measured under in-plane and perpendicular applied magnetic fields using a vibrating sample magnetometer (VSM) for each sample with a given Fe thickness. This allowed us to determine the saturation magnetic moment per unit area ($M_s \times t_{Fe}$) and then calculate the magnetization at saturation (M_s) and the thickness of the magnetic dead layer (t_d) for each system. To investigate iDMI and PMA versus temperature, BLS [13] in Damon-Eshbach configuration was employed to record spectra for a given field and spin wave vector (see Supplemental Material [14]). The temperature was varied from room temperature (RT) to 250° C and the spectra under an in-plane applied magnetic were recorded. Additionally, microstrip FMR (MSFMR) [15] was employed at room temperature and after temperature-variable BLS measurements to further study PMA and damping characteristics (see the Supplemental Material [14]).

III. RESULTS AND DISCUSSIONS

Room temperature measurements

This section is devoted for the RT static and dynamic magnetic properties. We first use VSM to measure the magnetization at saturation and determine the thickness of the magnetic dead layer. These are essential parameters for accurately calculating the PMA and interfacial DMI constants, as well as the efficiency of spin pumping. Subsequently, these parameters are examined and discussed to highlight the role of the two-magnon scattering contribution to magnetic damping and to isolate the role of each interface with Fe to the overall iDMI and interfacial PMA.

1. Static properties

Figure 1 shows the Fe thickness dependence of $M_s \times t_{Fe}$ for all the systems. The linear fits allow determining the magnetization at saturation and the thickness of the magnetic
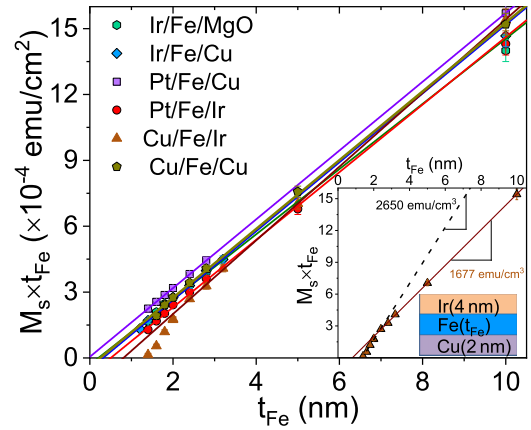

FIG. 1. Variation of the saturation magnetic moment per unit area versus the Fe thickness (t_{Fe}) for Fe-based systems with various buffer and capping layers grown on Si substrates. Symbols are VSM measurements and lines refer to the linear fits. The inset shows the corresponding data for Cu/Fe/Ir to illustrate the change of the slope of the linear dependence.

dead layer from the slope and the horizontal axis intercept, respectively. Table I summarizes the obtained values for M_s and t_d. One can note the absence of a magnetic dead layer for Pt/Fe/Cu and relatively low t_d values for Ir/Fe/MgO ($t_d = 0.2$ nm), Ir/Fe/Cu ($t_d = 0.32$ nm), and Cu/Fe/Cu ($t_d = 0.25$ nm). In contrast, higher t_d values are reported for Pt/Fe/Ir ($t_d = 0.5$ nm) and Cu/Fe/Ir ($t_d = 0.8$ nm), indicating that the thicker magnetic dead layers are associated with the presence of an Ir capping or buffer layer and with a Cu buffer layer. A simple basic analysis of t_d suggests an absence of a magnetic dead layer in Pt/Fe, minimal oxidation or intermixing at the Fe/MgO and Fe/Cu interfaces, and a significantly thicker magnetic dead layer at the Fe/Ir and Cu/Fe interfaces compared to those of Ir/Fe and Fe/Cu, respectively. This suggests greater interdiffusion at the Fe/Ir upper and Cu/Fe bottom interfaces. The M_s values listed in Table I are slightly lower than that of bulk Fe (1700 emu/cm^3) [16]. The values of M_s show minimal variation across the Ir/Fe/Cu, Pt/Fe/Cu, Pt/Fe/Ir, and Cu/Fe/Cu stacks; however, a decrease in M_s is noted for the Ir/Fe/MgO sample, likely due to oxygen penetration into Fe during MgO deposition [17]. In fact, the oxygen from the sputtered oxide layer (MgO) will migrate across the interface into the volume and will contaminate the Fe layer, similarly to the observed trend by Gweon *et al.* [17]. The latter used x-ray photoelectron spectroscopy to confirm the high level of oxygen contamination in Co of the as-grown Pt/Co/MgO sample compared to the annealed ones. Since the chemical affinity of oxygen and Fe is stronger than that with Co, we expect at least a similar trend.

The largest M_s value ($M_s = 1677$ emu/cm^3) was recorded for Cu/Fe/Ir. Notably, the slope of the thickness dependence of $M_s \times t_{Fe}$ for this system changes at a thickness of 2.4 nm (see the inset of Fig. 1). This suggests a change in M_s at a critical Fe thickness. Specifically, when using the thinner regime ($t_{Fe} \leqslant 2.4$ nm) for fitting, we obtain $t_d = 1.35$ nm and $M_s = 2650$ emu/cm^3, whereas the thicker range fitting gives $t_d = 0.85$ nm and $M_s = 1677$ emu/cm^3. This change of M_s could be attributed to a decrease in Curie temperature or

TABLE I. Parameters obtained from the best fits of the effective magnetization, the effective damping and the effective iDMI constants versus the inverse of the effective thickness of Fe thin films grown on Si substrates using various buffer and capping layers. "n.d." is used for "not determined."

System	M_s (emu/cm^3)	t_d (nm)	K_v (×10^5 J/m^3)	K_s (mJ/m^2)	α_0 (×10^{-3})	$g_{\text{eff}}^{\uparrow\downarrow}$ (nm^{-2})	β_{TM} (nm^2)	D_s (pJ/m)	ΔK_s (mJ/m^2)
Ir/Fe/MgO	1484	0.2	−0.93 ± 0.007	1.28 ± 0.02	2.1 ± 0.4	31.95 ± 2	n.d.	0.096 ± 0.003	0.36 ± 0.03
Ir/Fe/Cu	1568	0.32	−0.12 ± 0.001	1.02 ± 0.02	2 ± 0.2	29.88 ± 2	0.024 ± 0.003	0.27 ± 0.006	0.2 ± 0.02
Pt/Fe/Cu	1590	0	0.22 ± 0.002	0.87 ± 0.03	2 ± 0.3	19.18 ± 2	0.02 ± 0.003	−0.99 ± 0.04	0.2 ± 0.02
Pt/Fe/Ir	1540	0.5	−0.39 ± 0.002	1.09 ± 0.02	1.8 ± 0.2	49.37958 ± 3	n.d.	−1.28 ± 0.05	0.5 ± 0.03
Cu/Fe/Ir	1677	0.8	2.43 ± 0.02	1.49 ± 0.03	4 ± 0.4	35.14 ± 3	0.055 ± 0.005	−0.25 ± 0.006	0.2 ± 0.02
Cu/Fe/Cu	1566	0.25	1.59 ± 0.03	1.33 ± 0.07	5 ± 0.5	0	0.043 ± 0.005		

to a structural change during the growth. Indeed, structural differences, such as amorphous Fe for the thickest regime and (partially) textured polycrystalline Fe for the thinnest thickness regime may explain the change in M_s below and above a certain critical Fe thickness. Temperature dependence of $M_s \times t_{\text{Fe}}$ will be helpful to check whether the slope change also takes place at very low temperatures and therefore to identify the origin of this slope change. Although we have no direct evidence of such a structural change for these films, we believe that such structural changes for these thin films may occur at the first atomic planes. Indeed, this evolution of the structural and magnetic properties as a function of the Fe film thickness has been reported by Gubbiotti *et al.* [18], in Cu/Fe/Cu. They revealed that fcc pseudomorphic Fe layers, characterized by a low-spin ferromagnetic phase, grow to about 6 Å, while for larger thicknesses, they observed the appearance of three-dimensional bcc Fe (110) domains characterized by a high magnetic moment. For simplicity, all the measurements presented below for this system are analyzed by considering $M_s = 1677$ emu/cm^3 and $t_d = 0.8$ nm (parameters deduced from the fit of $M_s \times t_{\text{Fe}}$ of thick samples: above 2.4 nm). These values will be used to calculate PMA and iDMI parameters, and to explore the thickness influence on damping. It is also important to point out the superior quality of samples with the Pt underlayer, which benefits from the Ta seed layer. This latter reduces the induced roughness of the Si/SiO$_2$ substrate, as revealed by an atomic force microscope (not shown here). The Ta seed layer ensures thus a smoother atomic interface with Pt compared to Cu and Ir, thus enhancing the interface quality, reducing roughness, and significantly affecting magnetic properties.

2. PMA and damping

We will now first focus on the PMA and the Gilbert damping. To this end, MSFMR measurements were carried out following the procedure detailed in the Supplemental Material [14]. The effective magnetization (M_{eff} defined as $\mu_0 M_{\text{eff}} = \mu_0 M_s - \frac{2K_\perp}{M_s}$, where $K_\perp$ is the PMA constant) for all systems with the various capping and buffer layers is shown in Fig. 2 versus the inverse of the Fe effective thickness, defined as $t_{\text{eff}} = t_{\text{Fe}} - t_d$. One can observe a significant linear thickness dependence of $\mu_0 M_{\text{eff}}$ with a slope and a vertical intercept affected by the buffer and the capping layers, indicating an interfacial contribution to the PMA. Notably, there is a deviation from the linear behavior for the thinner Fe films, especially for Cu/Fe/Cu and Ir/Fe/Cu. This deviation from the linear

behavior is frequently reported for magnetic thin films. It could be attributed to interface degradation for thinner Fe, to coherent and incoherent growth of FM induced by the strain misfit of Fe and buffer or capping layers [19], to a decrease in the Curie temperature [20], or to the low thickness of the Fe layer that falls below the interface roughness and the depth of interdiffusion [21]. However, in our samples, it is most likely due to the interface quality degradation as the thickness is reduced. The linear dependence of $\mu_0 M_{\text{eff}}$ versus $1/t_{\text{eff}}$ suggests that $K_\perp$ can be described by the phenomenological relationship $K_\perp = K_v + \frac{K_s}{t_{\text{eff}}}$, where K_s and K_v are the perpendicular uniaxial surface and volume anisotropy constants, respectively. K_v and K_s are straightforwardly obtained from the vertical intercept and from the slope of the linear fit of $\mu_0 M_{\text{eff}}$ versus $1/t_{\text{eff}}$, as summarized in Table I. At this stage, it is a challenging task to precisely delineate the contribution of each interface with Fe to the total value of K_s presented in Table I, unless we assume that the interfaces with Fe involving the same material as a capping or buffer layer are symmetrical. Therefore, more information about K_s is required, and this specific contribution will be addressed later following the investigation of iDMI.
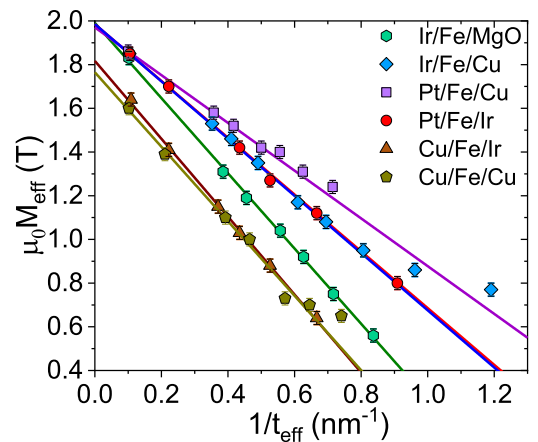

FIG. 2. Effective magnetization ($\mu_0 M_{\text{eff}}$) versus the Fe inverse effective thickness [$1/(t_{\text{Fe}} - t_d)$] for Fe-based systems with various buffer and capping layers grown on Si substrates. $\mu_0 M_{\text{eff}}$ values have been extracted from the fit of FMR measurements of the frequency of the uniform precession mode versus the in-plane applied magnetic field. Symbols refer to experimental data while solid lines are the linear fits taking into account only the thicker films.

As detailed in the Supplemental Material [14], the frequency dependences of the FMR field-sweep half linewidth at half maximum (ΔH) revealed a significantly different behavior for samples with the thicker Fe layers (10 nm). These samples exhibit a nonlinear variation of ΔH, while no obvious significant nonlinear contribution is observed for the thinner Fe films. This nonlinearity is attributed to two-magnon scattering (TMS) by the defects or dislocations [22–26] as confirmed by the out of plane angular dependence of ΔH and by the lower slope of the frequency dependence of ΔH when a perpendicular magnetic field is applied (refer to Fig. S2-3(c) and S2-4 in the Supplemental Material [14]). These perpendicular applied field linewidth measurements were feasible only for some few systems with thinner Fe films, due to the low signal to noise ratio in this configuration and the limited magnetic field strength available in our setup (see Supplemental Material [14]). The absence of the nonlinear behavior in the frequency dependence of ΔH for thinner Fe films, combined with the limitation in measuring ΔH under a perpendicular applied magnetic field, prevents a comprehensive fitting of ΔH that includes all contributions. Consequently, for the samples showing a linear behavior of ΔH, the linear fit is used to calculate the effective damping constant (α_{eff}). The variations of the effective damping constant α_{eff} as a function of $1/t_{\text{eff}}$ are shown in Fig. 3(a) for all systems. Two distinct trends emerge: while an almost linear dependence of α_{eff} versus $1/t_{\text{eff}}$ is revealed for Ir/Fe/MgO, a nonlinear behavior is observed for Cu/Fe/Ir, Cu/Fe/Cu, Pt/Fe/Cu, and Ir/Fe/Cu. Note the marked nonlinearity in the systems with a Cu buffer layer, indicating that TMS is the dominant relaxation mechanism for the thinnest films of the series. The highest damping values were obtained for Cu/Fe/Ir, suggesting a stronger TMS contribution, whereas the Pt/Fe/Cu system shows the lowest values. Furthermore, note the thickness dependence of α_{eff} of Cu/Fe/Cu where a negligible amount of spin pumping is expected, which further supports the role of the TMS mechanism in this behavior. This nonlinear behavior was also observed in the thickness dependence of the BLS mean linewidth of the Stokes and anti-Stokes lines, as shown in the Supplemental Material for Cu/Fe/Cu [see Figs. S4-3(a)] [14]. We thus conclude that the total damping in all the studied systems can be understood as the sum of the "intrinsic" damping (α_{Fe}) of the Fe layer and the interfacial damping, including spin pumping (characterized by a linear dependence with $1/t_{\text{eff}}$) and two-magnon scattering processes, given by $\alpha = \alpha_{\text{Fe}} + \alpha_P + \alpha_{\text{TM}}$. The spin pumping induced damping contribution is $\alpha_P = \frac{g\mu_B}{4\pi M_s t_{\text{eff}}} g_{\text{eff}}^{\uparrow\downarrow}$ (where μ_B is the Bohr magneton and $g_{\text{eff}}^{\uparrow\downarrow}$ is the effective spin mixing conductance) whereas $\alpha_{\text{TM}} = \frac{\beta_{\text{TM}}}{t_{\text{eff}}^2}$ is the interfacial TMS damping arising from the magnetic roughness. This interfacial two-magnon scattering is expected to be proportional to $\frac{1}{t_{\text{eff}}^2}$ because the two-magnon scattering scales with the square of the scattering potential, which is proportional to the inverse of the ferromagnetic film thickness [27].

The fits of the experimental data give α_{Fe}, β_{TM} (which parametrizes the strength of the TMS) and $g_{\text{eff}}^{\uparrow\downarrow}$ as summarized in Table I. For Pt/Fe/Ir and, in the lack of more experimental data, for thinner Fe layers (due to the weak MS-FMR signal due to the large damping values), evaluating β_{TM} is
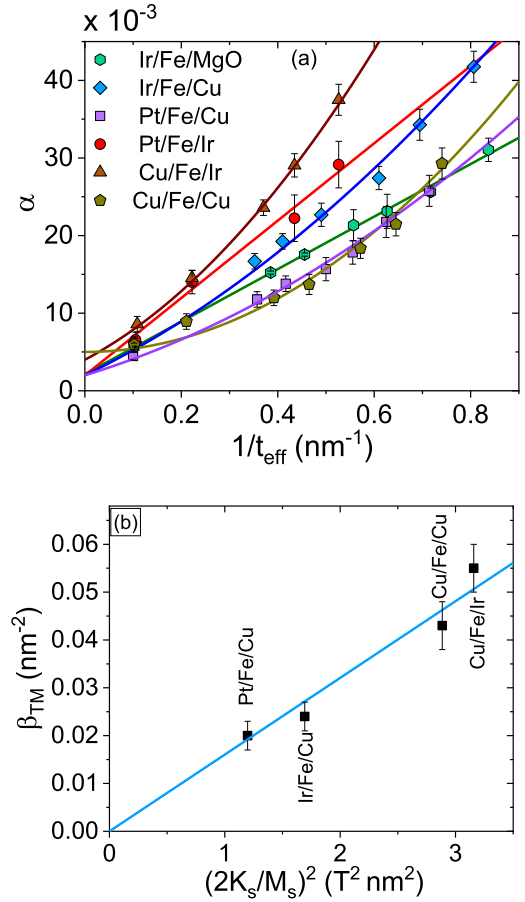

FIG. 3. (a) Effective magnetic damping parameter deduced from the in-plane applied magnetic field measurements, as a function of the inverse of the Fe effective thickness of the different studied systems. Symbols refer to the experimental data and solid lines are linear fits or fits using the model described in the main text. (b) Variation of the two-magnon scattering strength β_{TMS} versus $(\frac{2K_s}{M_s})^2$. Symbols refer to data deduced from fits of (a) and solid lines are linear fits.

a challenging task. β_{TM} is relatively large in Cu/Fe/Cu and Cu/Fe/Ir systems and comparatively lower for the other systems, reflecting its dependency on the surface conditions of ferromagnetic films such as the surface roughness and the surface magnetic anisotropy [28,29]. The variations of β_{TM} as a function of $(\frac{2K_s}{M_s})^2$ are shown in Fig. 3(b). A relatively good linear scaling is observed, in good agreement with the expectation for two-magnon scattering $\beta_{\text{TMS}} = C_{\text{TM}}(\frac{2K_s}{M_s})^2$ [30]. This finding suggests a consistency in the magnetic roughness of interfaces across different systems and establishes a correlation between β_{TM} and the interfacial magnetic anisotropy. It also confirms that the origin of the $\frac{1}{t_{\text{eff}}^2}$ dependence of the TMS damping is the distribution of the surface magnetic anisotropy due to interface defects as expected from the theory of Mills and co-workers (Lindner *et al.* [26] and Arias and Mills [28]). This is in good agreement with the higher ΔH_0 in a perpendicular applied magnetic field compared to the one measured in plane, attributed to interface PMA inhomogeneity. Furthermore, it is worth mentioning that the out of plane

angular dependence of ΔH cannot be fitted without taking into account the contribution resulting from the distribution of the effective magnetization (see Figs. S2–S2-4 in the Supplemental Material [14]). Furthermore, the obtained value of C_{TM} (0.016 T²) is very low compared to that of HM/FM/oxides (0.08 T²) [30] and the reported value (0.18 T²) by Yoshii *et al.* [31], suggesting variations in the strength of two-magnon scattering due to different interface characteristics. Note the weak two-magnon scattering of Ir/Fe/MgO despite the strength of both the spin-orbit coupling and the interfacial PMA in agreement with the observed behavior in Ta/Co/MgO [30]. It is worth mentioning the correlation between the thin magnetic dead layer and the strength of TMS: systems like Pt/Fe/Cu and Ir/Fe/MgO, where t_d is minimal, exhibit weak or even negligible TMS.

The thickness-independent damping of Fe (α_{Fe}) across all samples is consistently around 2×10^{-3}, in agreement with the reported value by Schoen *et al.* [32]. The higher α_{Fe} values of Cu/Fe/Ir and Cu/Fe/Cu are most likely effective damping values due to the strong two-magnon scattering in these systems, which leads to an overestimation of the intrinsic damping. Furthermore, as summarized in Table I, the $g_{eff}^{\uparrow\downarrow}$, a key parameter governing the spin-dependent transport through the HM/FM interface, exhibits slight differences between the Ir/Fe/Cu and Cu/Fe/Ir systems. This confirms again the asymmetry of Fe/Ir and Ir/Fe interfaces: the spin pumping efficiency is higher at the Fe/Ir interface. Given the negligible spin pumping at the Cu/Fe and Fe/MgO interfaces, it becomes clear that the $g_{eff}^{\uparrow\downarrow}$ at the Ir/Fe interface is substantially higher than at the Pt/Fe interface. The higher $g_{eff}^{\uparrow\downarrow}$ for Pt/Fe/Ir ($g_{eff}^{\uparrow\downarrow} = 49.37 \pm 3 \, \text{nm}^{-2}$) is in good agreement with the obtained values of Pt/Fe/Cu ($g_{eff}^{\uparrow\downarrow} = 19.18 \pm 2 \, \text{nm}^{-2}$) and Cu/Fe/Ir ($g_{eff}^{\uparrow\downarrow} = 35.14 \pm 3 \, \text{nm}^{-2}$).

3. Spin waves nonreciprocity and PMA

The iDMI constant for systems involving Pt and/or Ir was determined from the BLS measurements as detailed in the Supplemental Material [14]. Figure 4(a) shows a linear fit of the variation of the effective iDMI constant (D_{eff}) versus the inverse of the effective Fe thickness ($1/t_{eff}$), allowing the determination of the iDMI constant (D_s) for each system, as outlined in Table I. The analysis of the obtained values revealed that the iDMI constants of the Fe/Cu and Cu/Fe interfaces are negligible. Moreover, Pt/Fe and Ir/Fe interfaces have an opposite iDMI sign: it is positive for Ir/Fe and negative for Pt/Fe. Taking into account the D_s values of the different systems presented in Table I, we deduce $D_s^{Ir/Fe} = 0.27$ pJ/m, $D_s^{Pt/Fe} = -0.99$ pJ/m, and $D_s^{Fe/MgO} = -0.17$ pJ/m. This latter value is in good agreement with the value reported by Zhang *et al.* ($D_s^{Fe/MgO} = -0.15$ pJ/m) [33] and consistent with those of Co/MgO ($D_s^{Co/MgO} = -0.22$ pJ/m) [30] and CoFeB/MgO ($D_s^{CoFeB/MgO} = -0.17$ pJ/m) [34]. The obtained value of $D_s^{Ir/Fe}$ is also in good agreement with that of Co/Ir ($D_s^{Co/Ir} = 0.32$ pJ/m) [35] but slightly lower than the value reported by Zhang *et al.* [33] ($D_s \sim 0.6$ pJ/m) for iDMI measurements at room temperature on Ir/Fe(3 nm)/SiO₂. It is important to note that iDMI is sensitive to disorder, defects, and atom arrangement at the interfaces, which can significantly vary depending on the
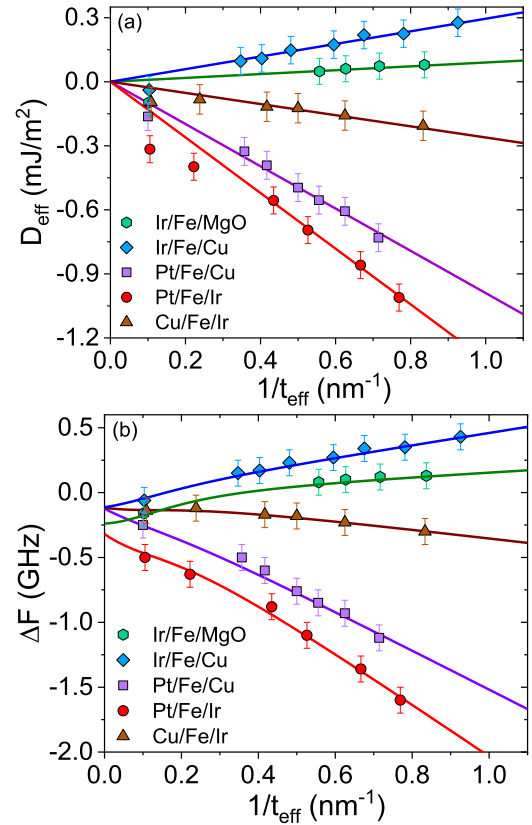

FIG. 4. Variation of (a) the effective iDMI constants and (b) the frequency shift between the Stokes and anti-Stokes lines (ΔF), measured at $k_{sw} = 20.45 \, \mu\text{m}^{-1}$ as a function of the Fe inverse effective thickness of Fe-based systems with various buffer and capping layers grown on Si substrates. Solid lines in (a) refer to the linear fits and symbols are experimental data. In (b), symbols are experimental data while solid lines refer to fits using equations given in the main text.

sample fabrication parameters, such as deposition technique and the choice of underlayer and capping layer materials. This variation often results in discrepancies between different experimentally obtained values of iDMI, due to differences in sample preparation and interfacial properties.

It is worth noting the deviation from the linear behavior of D_{eff} versus $1/t_{eff}$ for the thicker Fe films (above 2.8 nm), suggesting other contributions to ΔF. Furthermore, for the 10 nm thick Fe layer, ΔF is negative for all the systems despite the different sign of their total iDMI. Therefore, this nonlinearity cannot be due to iDMI. Indeed, the asymmetry of the PMA induced by the bottom and top FM interfaces is known to induce spin wave nonreciprocity [36]. Therefore, iDMI always combines with the effect of the interface PMA difference because both contributions to the spin wave frequency obey the same symmetry [36]. According to Gladii *et al.* [36], the frequency nonreciprocity due to the interface PMA difference scales linearly with the wave vector and quadratically with the FM thickness for thicknesses of 20 nm and below. Given that iDMI scales linearly with the inverse of FM thickness, ΔF of the thicker Fe layers ($t_{Fe} > 2.8$ nm) results mostly from the difference in interfacial PMA between the lower and upper interfaces while it is induced by iDMI for the thinner Fe films. To separate the two contributions, we first consider ΔF of the

TABLE II. Interface anisotropy constants for the different interfaces with Fe obtained from the combination of ΔK_s and K_s values indicated in Table I.

$K_s^{Fe/Cu}$ (mJ/m^2)	$K_s^{Cu/Fe}$ (mJ/m^2)	$K_s^{Pt/Fe}$ (mJ/m^2)	$K_s^{Fe/Ir}$ (mJ/m^2)	$K_s^{Fe/MgO}$ (mJ/m^2)	$K_s^{Ir/Fe}$ (mJ/m^2)
0.57 ± 0.04	0.65 ± 0.05	0.29 ± 0.04	0.8 ± 0.05	0.82 ± 0.05	0.43 ± 0.03

thinner samples ($t_{Fe} < 2.8$ nm) for each sample to determine D_{eff} and then D_s as indicated in Table I. The entire range of t_{Fe} variations in ΔF was then modeled using the following equation, $\Delta F = D_s \frac{4\gamma}{2\pi M_s t_{eff}} k_{sw} + \frac{8\gamma}{\pi^3} \frac{K_s^{bot} - K_s^{top}}{M_s} \frac{1}{1 + \frac{\Delta^2 \pi^2}{t_{eff}^2}} k_{sw}$, where $\Delta = \sqrt{\frac{2A_{ex}}{\mu_0 M_s}}$ is the exchange length and $\Delta K_s = K_s^{top} - K_s^{bot}$ is the difference in surface anisotropies of the top and the bottom interfaces with Fe [see Fig. 4(b)]. This model allows for fitting using ΔK_s as a parameter, as presented in Table I. Note the positive sign of ΔK_s and thus the higher surface anisotropy induced by the top interface with Fe for all the systems.

To accurately separate the contribution of each interface with Fe to PMA, we combined the interface PMA constant's difference between the top and bottom interfaces ($\Delta K_s = K_s^{top} - K_s^{bot}$) with the effective interface PMA constant ($K_s = K_s^{top} + K_s^{bot}$), values indicated in Table I. The obtained values for each interface are summarized in Table II. The calculated values for Cu/Fe and Fe/Cu allowed evaluating the effective interface anisotropy constant of Cu/Fe/Cu ($K_s = K_s^{Cu/Fe} + K_s^{Fe/Cu} = 0.65 + 0.57 = 1.22$ mJ/m^2). The obtained value is in good agreement with the one obtained directly from the fit of the thickness dependence of M_{eff} of this system, given in Table I. Significant asymmetry in the interface PMA constants was observed for Fe/Ir and Ir/Fe, while a lesser extent is recorded for Fe/Cu and Cu/Fe. The interfaces involving Fe/MgO and Fe/Ir exhibit the strongest interface anisotropies. In contrast, the Pt/Fe interface demonstrated relatively weak interface anisotropy.

IV. TEMPERATURE DEPENDENCE MEASUREMENTS

In this section, we will focus on the effect of the measurement temperature on PMA, iDMI, and damping of Cu/Fe/Cu and Pt/Fe/Cu systems. The choice of Pt/Fe/Cu is driven by the significant iDMI induced by the single Pt/Fe interface, while Cu/Fe/Cu serves as a reference system that exhibits both TMS and interface PMA. It is worth mentioning that our VSM setup does not allow temperature dependence measurements and, therefore, for each temperature we will consider M_s values at room temperature (RT) for the analysis of data as a function of temperature. This approach is justifiable considering the high Curie temperature of Fe (1044 K) [37] and the low measurement temperatures of this study ($\leqslant 250\,^{\circ}$C). Under these conditions, the change in M_s is less than 6%. Furthermore, in the absence of VSM measurements for each temperature, we rely on t_d values of the as-grown samples to evaluate the effective Fe thickness used in the analysis of the experimental data.

The temperature dependences of K_s and D_s for the Pt/Fe/Cu system reveal distinct behaviors, as shown in Figs. 5(a) and 5(b). K_s exhibits a linear increase across the entire temperature range up to $250\,^{\circ}$C, with an overall increase of about 20%. In contrast, D_s demonstrates a pronounced nonlinear decrease

with temperature, decreasing in absolute value by approximately 60%. This significant variation suggests that iDMI is markedly more sensitive to temperature changes compared to PMA and M_s. This finding aligns with observations made by Schlotter *et al.* [38], who reported that interfacial iDMI varies more strongly with temperature than PMA and M_s. This variation of iDMI with temperature cannot be due to the weak M_s change in the range of RT, 250 °C. As mentioned above, interface anisotropy results mainly from the Fe/Cu interface, whereas iDMI is induced by the Pt/Fe interface. This could explain the difference in behavior between K_s and D_s, suggesting that the Pt/Fe interface is more affected by the temperature during the measurement. In addition, at high temperatures, oxidation can also take place because samples are heated in air, leading to a reduction in M_s and may be responsible for the anisotropy increase.

The investigation of the correlation between iDMI and PMA is particularly insightful for understanding the interaction dynamics at magnetic interfaces and designing a system with the desired properties. Ideally, this correlation could be investigated by studying the variation of K_s as a function of D_s as shown in Fig. 5(c). While a linear relationship can be fitted to the data, a second-order polynomial fit provides a better fit of the experimental data. This could be due to the greater sensitivity of iDMI compared to interface anisotropy. Furthermore, iDMI results mainly from the Pt/Fe interface, whereas K_s is induced by the Pt/Fe interfaces and predominantly by Fe/Cu which seems to be less affected by temperature, hence the low variation. It is worth mentioning that both K_s and D_s calculations involve a linear dependence of M_s. Therefore, their correlation is less affected by the
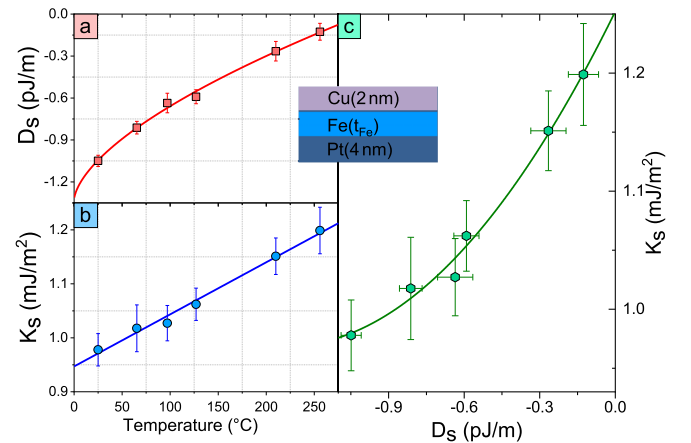

FIG. 5. Temperature dependence of (a) the surface iDMI and (b) the interface PMA constants of the Pt/Fe/Cu samples grown on Si substrates. (c) Corresponding variation of the interface PMA versus the surface iDMI constants traducing their ccorrelation. Solid lines refer to fits (linear or nonlinear) and symbols are experimental data.
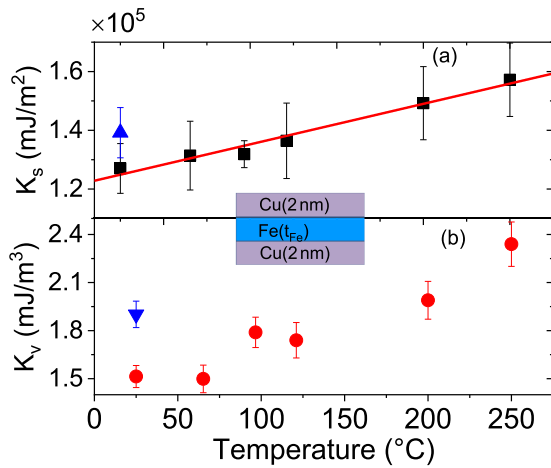
FIG. 6. Variations of the perpendicular (a) interface and (b) volume anisotropy constants of the Cu/Fe/Cu system as a function of temperature. The blue triangles represent values obtained after a complete temperature measurement cycle. The obtained values were deduced from BLS measurements.

incertitude on M_s, which thus overcomes the need to measure M_s as a function of temperature. Similar behaviors have been observed for the temperature dependence of both K_s and K_v of Cu/Fe/Cu systems (see Fig. 6) with a slightly smaller slope of K_s (1×10^{-3} mJ/m$^2\,$°C) compared to that of Pt/Fe/Cu (1.4×10^{-3} mJ/m$^2\,$°C). The temperature dependence of the Stokes and anti-Stokes mean linewidths, measured at a magnetic field of 0.2 T (see Fig. S4-2(a) in the Supplemental Material [14]) revealed an irreversible increase, suggesting a structural evolution during heating, resulting from inter-diffusion. The latter occurs mainly at the bottom interface, confirming the weak variation of K_s of Pt/Fe/Cu with temperature.

Several underlying mechanisms could be responsible for the observed behavior of anisotropy and iDMI as a function of temperature. As temperature increases, there might be evolution of the crystal structure during the measurements coupled to atomic diffusion and lattice strain at the interfaces. These changes can alter the local magnetic environment, thereby affecting both K_s and D_s. The thermal expansion contributes to lattice strain and could play a role in this behavior in the same way that thermal expansion of the lattice is a primary source of the temperature dependence of the Heisenberg exchange [39]. Moreover, using the extended droplet model, Kim *et al.* [40] found that the iDMI increases with decreasing temperature in a range from 300 to 100 K. Since the electron-phonon interaction promotes, in general, thermally induced hopping between nearest neighbors, when increasing the temperature, it is expected that the difference between in-plane and out of plane hopping energies is reduced upon temperature increase, leading to a redistribution of charge between the orbitals and potentially affecting the iDMI. Furthermore, the electron-phonon interactions and magnetization fluctuations lead to a broadening of the Fermi energy, affecting thus the temperature behavior of iDMI [40]. Finally, this temperature dependence, in particular that of D_s, could be due to the hybridization of 3d and 5d orbitals near the Fermi level and thermal disorder. As will be discussed below and in the
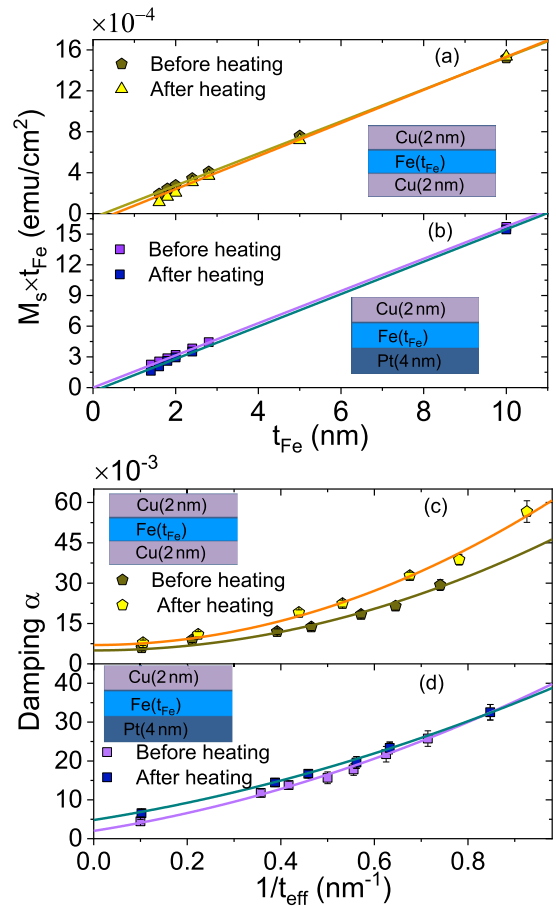

FIG. 7. Variation of the saturation magnetic moment per unit area versus the Fe thickness for (a) Cu/Fe/Cu and (b) Pt/Fe/Cu samples before and after a complete temperature measurement cycle (room temperature to 250° C). Symbols are VSM measurements and lines refer to the linear fits. Effective magnetic damping parameter as a function of the inverse of for (c) Cu/Fe/Cu and (d) Pt/Fe/Cu samples before and after a complete temperature measurement cycle. Symbols refer to the experimental data and solid lines are fits using the model described in the paper text.

Supplemental Material [14], the crystal structural evolution of Pt/Fe/Cu during the temperature-dependent measurements cannot induce such large variation of D_s and we can conclude that electron-phonon interactions are the main source of the temperature dependence of D_s. The temperature dependence of M_s will be helpful to obtain the scaling of D_s with M_s and, therefore, to get further insights into the origin of the thermal dependence of the iDMI constant.

To assess the impact of temperature on the structural and magnetic properties of Pt/Fe/Cu and Cu/Fe/Cu samples, MSFMR was employed to determine the PMA constants and the magnetic damping coefficient after a complete cycle of temperature measurements. The obtained values were then compared with those deduced from MSFMR measurements on the same samples before proceeding to temperature-dependent measurements. Figures 7(a) and 7(b) show the thickness dependences of the magnetic moment per unit area of as-grown samples Pt/Fe/Cu and Cu/Fe/Cu (before heating) compared to those that have undergone a complete

temperature measurement cycle (after heating). Both systems exhibited an increase in the thickness of the magnetic dead layer, 0.22 nm for Pt-buffered samples and 0.52 nm for Cu-buffered samples. These observations suggest a significant interdiffusion that occurs at the Fe interfaces during the temperature measurement process. Indeed, as the temperature rises, interdiffusion is triggered and becomes more pronounced as the measurement time increases. This results in an intermixing of the interface atoms at and, consequently, the formation of a magnetic dead layer. Determining the precise factors governing the mixing between atoms at interfaces can be challenging. However, it appears that the atomic radius and electronegativity of the atoms play crucial roles in facilitating this phenomenon [41,42]. Note the slope change at $t_{Fe} = 2.4$ nm for Cu/Fe/Cu after heating in a manner similar to the above-discussed trend. This suggests that this change of M_s at a critical thickness of Fe is most probably due to the structural enhancement of these thin films resulting from the prolonged exposure to increased temperature. This is in good agreement with the slight increase in M_s after heating ($M_s = 1618$ emu/cm^3 and $M_s = 1583$ emu/cm^3 for Cu/Fe/Cu and Pt/Fe/Cu, respectively).

The linear fitting of the thickness dependences of M_{eff} and iDMI constant (see Figs. S4-2(b), S4-2(c), and S4-3(b) in the Supplemental Material [14]), as well as the damping fitting with the above-mentioned model taking into account the TMS contribution were used to obtain K_s, K_v, $g_{eff}^{\uparrow\downarrow}$, β_{TM}, and D_s for both systems [see Figs. 7(c) and 7(d)]. The obtained values of PMA constants (from the MSFMR measurements) for Pt/Fe/Cu, before [$K_s = 0.86 \pm 0.03$ mJ/m^2 and $K_v = (0.22 \pm 0.002) \times 10^5$ J/m^3] and after a complete heating process [$K_s = 0.84 \pm 0.03$ mJ/m^2 and $K_v = (0.69 \pm 0.006) \times 10^5$ J/m^3], show that only the volume anisotropy is significantly changed. Furthermore, the obtained values for the Fe damping, β_{TM} and iDMI constant after heating are found to be $\alpha_{Fe} = 4.8 \times 10^{-3}$, $\beta_{TM} = 1.6 \times 10^{-2}$ nm^2, $g_{eff}^{\uparrow\downarrow} = 19.1$ nm^{-2}, and $D_s = -0.8$ pJ/m (see Fig. S4-3(b) in the Supplemental Material [14]). α_{Fe} is considerably higher than the one obtained before heating, most probably due to the atomic interdiffusion. Indeed the presence of impurities, especially those with large spin-orbit coupling, considerably degrades (increases) the damping of a magnetic material [43,44]. In contrast to the other interface parameters (K_s and $g_{eff}^{\uparrow\downarrow}$), D_s and β_{TM} have decreased slightly after heating, again suggesting the stronger temperature dependence of iDMI compared to K_s and $g_{eff}^{\uparrow\downarrow}$. These temperature-dependent measurements result in a significant change in the bulk magnetic properties, such as the volume anisotropy and damping constants after heating, while interface properties are less affected. In the case of Cu/Fe/Cu, the obtained values for K_s and K_v (from the BLS measurements) are shown in Fig. 6 in blue triangles, indicating a slight increase compared to those measured prior to heating. The deduced PMA constants from the FMR measurements (see Figs. S4-2a and S4-2c in the Supplemental Material [14]), found to be [$K_s = 1.33 \pm 0.07$ mJ/m^2 and $K_v = (1.59 \pm 0.03) \times 10^5$ J/m^3] before and [$K_s = 1.37 \pm 0.1$ mJ/m^2 and $K_v = (1.91 \pm 0.07) \times 10^5$ J/m^3] after a complete heating process are in good agreement with those obtained from BLS. Moreover, besides the increase of Fe damping (α_{Fe} increases from 5×10^{-3} to 7×10^{-3}), a sig-

nificant increase of β_{TM} ($\beta_{TM} = 5.6 \times 10^{-2}$ nm^2) is obtained after heating, probably due to the interdiffusion that occurs at interfaces with Cu. This interfacial TMS contribution has been also been confirmed by the BLS measurements of thickness dependence of the mean linewidth of Stokes and anti-Stokes lines as shown in the Supplemental Material for Cu/Fe/Cu [refer to Fig. S4-3(a)] [14].

It is worth stating that we think that the effect of the temperature on magnetic properties is twofold: structural evolution (irreversible) such as atomic diffusion, which has a greater effect on volume properties, and a pure temperature effect via one of the above-mentioned mechanisms, whose effect on interface properties is greater and more visible. Furthermore, the BLS temperature-dependent measurements above room temperature seem to be difficult to explain and analyze given the prolonged exposure of samples to temperature, imposed by the long accumulation times in BLS, which will also have an effect similar to annealing. Therefore, quicker techniques for such temperature measurements are needed.

V. CONCLUSION

We conducted a comprehensive study on the interfacial magnetic properties of Fe-based systems with various capping and buffer layers. Our research demonstrates the feasibility of distinguishing the individual interface contributions to the perpendicular magnetic anisotropy. This can be achieved by combining the analysis of the effective interface constants and the differences in interface anisotropy between the top and bottom interfaces with Fe. These parameters were derived from the thickness dependencies of effective magnetization and the spin wave frequency mismatch in thicker Fe films. The FMR linewidth measurements under an in-plane applied magnetic field revealed the presence of an additional extrinsic damping caused by the interfacial two-magnon scattering, which was correlated with interface magnetic anisotropy. Furthermore, the thickness dependence of the effective interfacial Dzyaloshinskii-Moriya interaction (iDMI) constant was investigated, allowing for the separation of contributions from the various interfaces. Notably, the Ir/Fe and Fe/MgO interfaces induce weak iDMI of opposite signs, contributing to the total iDMI. We also assessed the temperature dependence of iDMI, damping, and interface PMA in Pt/Fe/Cu and Cu/Fe/Cu thin films, key factors for potential spintronic applications. Our findings revealed an increase of both damping and PMA constant with temperature and a significant decrease of iDMI due to the enhanced thermal fluctuations. These observations underscore the heightened sensitivity of iDMI to temperature changes, raising important further considerations regarding the specific mechanisms driving the temperature dependence of iDMI and the influence of structural changes on its behavior.

[1] A. Soumyanarayanan, N. Reyren, A. Fert, and C. Panagopoulos, Emergent phenomena induced by spin-orbit coupling at surfaces and interfaces, Nature (London) **539**, 509 (2016).

[2] P. M. Haney and M. D. Stiles, Current-induced torques in the presence of spin-orbit coupling, Phys. Rev. Lett. **105**, 126602 (2010).

[3] M. T. Johnson, R. Jungblut, P. J. Kelly, and F. J. A. den Breeder, Perpendicular magnetic anisotropy of multilayers: Recent insights, J Magn. Magn. Mater. **148**, 118 (1995).

[4] B. Dieny and M. Chshiev, Perpendicular magnetic anisotropy at transition metal/oxide interfaces and applications, Rev. Mod. Phys. **89**, 025008 (2017).

[5] R. H. Zhao, Z. Y. Ren, J. P. Cao, Y. S. Yuan, G. L. Zhao, X. G. Xu, K. K. Meng, J. Miao, and Y. Jiang, Influence of heavy-metal capping layers on perpendicular magnetic anisotropy and spin-orbit torques of Pt/Co/HM stacks structures, Solid State Comm. **332**, 114340 (2021).

[6] Y. Tserkovnyak, A. Brataas, and G. E. W. Bauer, Enhanced Gilbert damping in thin ferromagnetic films, Phys. Rev. Lett. **88**, 117601 (2002).

[7] M. Shen, X. Li, Y. Zhang, X. Yang, and S. Chen, Effects of the interfacial Dzyaloshinskii–Moriya interaction on magnetic dynamics, J. Phys. D: Appl. Phys. **55**, 213002 (2022).

[8] J. Sinova, S. O. Valenzuela, J. Wunderlich, C. H. Back, and T. Jungwirth, Spin Hall effects, Rev. Mod. Phys. **87**, 1213 (2015).

[9] D. Mancilla-Almonacid, R. Jaeschke-Ubiergo, A. S. Núñez, and S. Allende, Ultrafast domain wall propagation due to the interfacial Dzyaloshinskii–Moriya interaction, Nanotechnology **31**, 125707 (2020).

[10] F. Ma and Y. Zhou, Interfacial Dzialoshinskii–Moriya interaction induced nonreciprocity of spin waves in magnonic waveguides, R. Soc. Chem. Adv. **4**, 46454 (2014).

[11] H. Yang, A. Thiaville, S. Rohart, A. Fert, and M. Chshiev, Anatomy of Dzyaloshinskii-Moriya interaction at interfaces, Phys. Rev. Lett. **115**, 267210 (2015).

[12] J. Cho, N-H. Kim, S. Lee, J-S. Kim, R. Lavrijsen, A. Solignac, Y. Yin, D-S. Han, N. J. J. van Hoof, H. J. M. Swagten, B. Koopmans, and C-Y. You, Thickness dependence of the interfacial Dzyaloshinskii–Moriya interaction in inversion symmetry broken systems, Nat. Commun. **6**, 7635 (2015).

[13] M. Belmeguenai, M. S. Gabor, Y. Roussigné, A. Stashkevich, S. M. Chérif, F. Zighem, and C. Tiusan, Brillouin light scattering investigation of the thickness dependence of Dzyaloshinskii-Moriya interaction in $Co_{0.5}Fe_{0.5}$ ultrathin films, Phys. Rev. B **93**, 174407 (2016).

[14] See Supplemental Material at http://link.aps.org/supplemental/10.1103/PhysRevB.109.214426 for more details about sample structure and BLS and FMR measurements, as well as for temperature-dependent measurement setup and data, which includes Refs. [45–51].

[15] M. Belmeguenai, M. S. Gabor, F. Zighem, N. Challab, T. Petrisor Jr., R. B. Mos, and C. Tiusan, Ferromagnetic-resonance-induced spin pumping in $Co_{20}Fe_{60}B_{20}$/Pt systems: Damping investigation, J. Phys. D: Appl. Phys. **51**, 045002 (2018).

[16] J.-M. L. Beaujour, A. D. Kent, D. W. Abraham, and J. Z. Sun, Ferromagnetic resonance study of polycrystalline $Fe_{1-x}V_x$ alloy thin films, J. Appl. Phys. **103**, 07B519 (2008).

[17] H. K. Gweon, S. J. Yun, and S. H. Lim, A very large perpendicular magnetic anisotropy in Pt/Co/MgO trilayers fabricated by controlling the MgO sputtering power and its thickness, Sci. Rep. **8**, 1266 (2018).

[18] G. Gubbiotti, L. Albini, S. Tacchi, G. Carlotti, R. Gunnella, and M. De Crescenzi, Structural and magnetic properties of epitaxial Cu/Fe/Cu/Si(111) ultrathin films, Phys. Rev. B **60**, 17150 (1999).

[19] M. T. Johnson, P. J. H. Bloemenz, F. J. A. den Broeder, and J. J. de Vries, Magnetic anisotropy in metallic multilayers, Rep. Prog. Phys. **59**, 1409 (1996).

[20] C. J. Lin, G. L. Gorman, C. H. Lee, R. F. C. Farrow, E. E. Marinero, H. V. Do, H. Notarys, and C. J. Chien, Magnetic and structural properties of Co/Pt multilayers, J. Magn. Magn. Mater. **93**, 194 (1991).

[21] W. B. Zeper, F. J. A. M. Greidanus, P. F. Carcia, and C. R. Fincher, Perpendicular magnetic anisotropy and magneto-optical Kerr effect of vapor-deposited Co/Pt-layered structures, J. Appl. Phys. **65**, 4971 (1989).

[22] R. D. McMichael, D. J. Twisselmann, and A. Kunz, Localized ferromagnetic resonance in inhomogeneous thin films, Phys. Rev. Lett. **90**, 227601 (2003).

[23] M. J. Hurben and C. E. Patton, Theory of two magnon scattering microwave relaxation and ferromagnetic resonance linewidth in magnetic thin films, J. Appl. Phys. **83**, 4344 (1998).

[24] J. Lindner, K. Lenz, E. Kosubek, K. Baberschke, D. Spoddig, R. Meckenstock, J. Pelzl, Z. Frait, and D. L. Mills, Non-Gilbert-type damping of the magnetic relaxation in ultrathin ferromagnets: Importance of magnon-magnon scattering, Phys. Rev. B **68**, 060102(R) (2003).

[25] S. Wu, D. A. Smith, P. Nakarmi, A. Rai, M. Clavel, M. K. Hudait, J. Zhao, F. M. Michel, C. Mewes, T. Mewes, and S. Emori, Room-temperature intrinsic and extrinsic damping in polycrystalline Fe thin films, Phys. Rev. B **105**, 174408 (2022).

[26] J. Lindner, I. Barsukov, C. Raeder, C. Hassel, O. Posth, R. Meckenstock, P. Landeros, and D. L. Mills, Two-magnon damping in thin films in case of canted magnetization: Theory versus experiment, Phys. Rev. B **80**, 224421 (2009).

[27] J. Beik Mohammadi, J. M. Jones, S. Paul, B. Khodadadi, C. K. A. Mewes, T. Mewes, and C. Kaiser, Broadband ferromagnetic resonance characterization of anisotropies and relaxation in exchange-biased IrMn/CoFe bilayers, Phys. Rev. B **95**, 064414 (2017).

[28] R. Arias and D. L. Mills, Extrinsic contributions to the ferromagnetic resonance response of ultrathin films, Phys. Rev. B **60**, 7395 (1999).

[29] A. Azevedo, A. B. Oliveira, F. M. de Aguiar, and S. M. Rezende, Extrinsic contributions to spin-wave damping and renormalization in thin films, Phys. Rev. B **62**, 5331 (2000).

[30] L. Zhu, L. Zhu, D. C. Ralph, and R. A. Buhrman, Origin of strong two-magnon scattering in heavy-metal/ferromagnet/oxide heterostructures, Phys. Rev. Appl. **13**, 034038 (2020).

[31] S. Yoshii, K. Kato, E. Shigematsu, R. Ohshima, Y. Ando, K. Usami, and M. Shiraishi, Significant suppression of two-magnon scattering in ultrathin Co by controlling the surface magnetic anisotropy at the Co/nonmagnet interfaces, Phys. Rev. B **106**, 174414 (2022).

[32] M. A. W. Schoen, D. Thonig, M. L. Schneider, T. J. Silva, H. T. Nembach, O. Eriksson, O. Karis, and J. M. Shaw, Ultra-low magnetic damping of a metallic ferromagnet, Nat. Phys. **12**, 839 (2016).

[33] W. Zhang, B. Jiang, L. Wang, Y. Fan, Y. Zhang, S. Y. Yu, G. B. Han, G. L. Liu, C. Feng, G. H. Yu, S. S. Yan, and S. Kang, Enhancement of interfacial Dzyaloshinskii-Moriya interaction: A comprehensive investigation of magnetic dynamics, Phys. Rev. Appl. **12**, 064031 (2019).

[34] X. Ma, G. Yu, C. Tang, X. Li, C. He, J. Shi, K. L. Wang, and X. Li, Interfacial Dzyaloshinskii-Moriya interaction: Effect of 5*d* band filling and correlation with spin mixing conductance, Phys. Rev. Lett. **120**, 157204 (2018).

[35] I. Benguettat-El Mokhtari, D. Ourdani, Y. Roussigné, R. B. Mos, M. Nasui, F. Kail, L. Chahed, S. M. Chérif, A. Stashkevich, M. Gabor, and M. Belmeguenai, Perpendicular magnetic anisotropy and interfacial Dzyaloshinskii–Moriya interaction in as grown and annealed *X*/Co/*Y* ultrathin systems, J. Phys.: Condens. Matter **32**, 495802 (2020).

[36] O. Gladii, M. Haidar, Y. Henry, M. Kostylev, and M. Bailleul, Frequency nonreciprocity of surface spin wave in permalloy thin films, Phys. Rev. B **93**, 054430 (2016).

[37] J. Crangle and G. M. Goodman, The magnetization of pure iron and nickel, Proc. R. Soc. London, Ser. A **321**, 477 (1971).

[38] S. Schlotter, P. Agrawal, and G. S. D. Beach, Temperature dependence of the Dzyaloshinskii-Moriya interaction in Pt/Co/Cu thin film heterostructures, Appl. Phys. Lett. **113**, 092402 (2018).

[39] T. Brawell, Temperature dependence of the isotropic exchange constant, J Phys.: Condens. Matter **2**, 7527 (1990).

[40] S. Kim, K. Ueda, G. Go, P-H. Jang, K-J. Lee, A. Belabes, A. Manchon, M. Suzuki, Y. Kotani, T. Nakamura, K. Nakamur, T. Koyama, D. Chiba, K. T. Yamada, D-H. Kim, T. Moriyama, K.-J. Kim, and T. Ono, Correlation of the Dzyaloshinskii–Moriya interaction with Heisenberg exchange and orbital asphericity, Nat. Commun. **9**, 1648 (2018).

[41] T. Nakayama, S. Itaya, and D. Murayama, Nano-scale view of atom intermixing at metal/semiconductor interfaces, J Phys.: Conf. Ser. **38**, 216 (2006).

[42] D. C. Ghosh, A new scale of electronegativity based on absolute radii of atoms, J. Theor. Comput. Chem. **04**, 21 (2005).

[43] J. O. Rantschler, R. D. McMichael, A. Castillo, A. J. Shapiro, W. F. Egelhoff Jr., B. B. Maranville, D. Pulugurtha, A. P. Chen, and L. M. Connors, Effect of 3*d*, 4*d*, and 5*d* transition metal doping on damping in permalloy thin films, J Appl. Phys. **101**, 033911 (2007).

[44] T. Devolder, S. Couet, J. Swerts, and G. S. Kar, Gilbert damping of high anisotropy Co/Pt multilayers, J. Phys. D: Appl. Phys. **51**, 135002 (2018).

[45] D. Ourdani, Y. Roussigné, S. M. Chérif, M. S. Gabor, and M. Belmeguenai, Thickness dependence of magnetic properties of Ir/FeV-based systems, Phys. Rev. Mater. **7**, 034408 (2023).

[46] W. K. Peria, T. A. Peterson, A. P. McFadden, T. Qu, C. Liu, C. J. Palmstrøm, and P. A. Crowell, Interplay of large two-magnon ferromagnetic resonance linewidths and low Gilbert damping in Heusler thin films, Phys. Rev. B **101**, 134430 (2020).

[47] S. Mizukami, D. Watanabe, M. Oogane, Y. Ando, Y. Miura, M. Shirai, and T. Miyazaki, Low damping constant for Co_2FeAl Heusler alloy films and its correlation with density of states, J. Appl. Phys. **105**, 07D306 (2009).

[48] P. Krivosik, N. Mo, S. Kalarickal, and C. E. Patton, Hamiltonian formalism for two magnon scattering microwave relaxation: Theory and applications, J. Appl. Phys. **101**, 083901 (2007).

[49] R. D. McMichael, M. D. Stiles, P. J. Chen, and W. F. Egelhoff Jr., Ferromagnetic resonance linewidth in thin films coupled to NiO, J. Appl. Phys. **83**, 7037 (1998).

[50] N. Mo, J. Hohlfeld, M. ul Islam, C. S. Brown, E. Girt, P. Krivosik, W. Tong, A. Rebei, and C. E. Patton, Origins of the damping in perpendicular media: Three component ferromagnetic resonance linewidth in Co–Cr–Pt alloy films, Appl. Phys. Lett. **92**, 022506 (2008).

[51] D. Ourdani, Y. Roussigné, S. M. Chérif, M. S. Gabor, and M. Belmeguenai, Correlation between interface perpendicular magnetic anisotropy and interfacial Dzyaloshinskii–Moriya interactions in Pt/Pd (*t*Pd)/Co (*t*Co)/Au, J. Phys. D: Appl. Phys. **55**, 485004 (2022).